Expansion of SYS Cam-clay model for simulation of mechanical behavior of cement-treated soils

Expansion du modèle SYS Cam-clay pour la simulation du comportement mécanique du ciment-traité sols

Shotaro Yamada & Masaki Nakano
Civil and Environmental Engineering, Nagoya University, Japan, s-yamada@civil.nagoya-u.ac.jp

ABSTRACT: Asaoka et al. (2002) proposed an elasto-plastic constitutive model, the SYS Cam-clay model, based on the soil skeleton structure concept as a constitutive equation which can reproduce the mechanical behavior of naturally deposited clays. This paper expanded the model to describe the mechanical behavior of cement-treated soils based on element experiments and demonstrated high reproduction capability of the proposed model.

RÉSUMÉ: Asaoka et al. (2002) ont proposé un modèle constitutif élasto-plastique, le modèle SYS Cam-clay, basée sur la structure concept de squelette du sol comme une équation constitutive qui peut reproduire le comportement mécanique des argiles naturellement déposées. Ce document a élargi le modèle pour décrire le comportement mécanique des sols de ciment-traité basé sur des expériences d'éléments et démontré une capacité élevée de reproduction du modèle proposé.

KEYWORDS: cement-treated soil, elasto-plastic constitutive model, modified stress.

1 INTRODUCTION

Asaoka et al. (2002) proposed the SYS Cam-clay model, which was an elasto-plastic constitutive model based on a soil skeleton structure concept. The model can reproduce the mechanical behavior of naturally deposited clays. This paper addresses the expansion of the model so that it can describe the mechanical behavior of cement-treated soils. To that end, this study firstly identifies similarities and distinctions between cement-treated soils and naturally deposited clays by comparing with element experiments for both soils. Secondly, briefing on the expansion is followed by formulation of the proposed model. Finally, some element tests for a cement-treated soil are simulated by using the proposed model in order to validate it.

2 ELEMENT TESTS FOR CEMENT-TREATED SOIL

In this section, mechanical features of cement treated soils will be revealed through comparison element experiments for a cement treated soil with that for a naturally deposited clay.

2 .1 *Physical property of base material and blending condition of cement-treated soil*

Clay dredged from the *Yuraku-cho* layer in Tokyo bay area was used as the base material. The clay content and silt content of the dredged clay are 60 and 40%, respectively. The liquid limit w_L and the plastic limit w_P of the dredged clay are 91.2 and 39.0%, respectively. A blending condition was decided on the assumption that the pneumatic flow mixing method (Coastal Development Institute of Technology, 2008) was applied to the dredged clay. The target flow value was set from 90 to 100mm and the target unconfined strength at 28 curing days was set from 100 to 200kPa. Table 1 shows the blending condition that satisfies the above condition. The water content of dredged clay w_0 is the water content before blending cement. S, W and C in the table represent the mass of soil particles, water and cement contained in the saturated treated soil 1m^3, respectively.

Table 1. Blending condition.

Water content of dredged soil w_0 (%)	Cement dosage C (kg/m^3)	Water-cement ratio W/C	Soil-cement ratio S/C
170	50	16.1	9.47

2 .2 *Oedometer test*

Figure 1 shows oedometer test results for the treated soil and two kinds of remolded samples, which were produced by remolding the treated soil once solidified and by remolding the deposited clay under the water liquid limit. The state of the non-disturbed treated soil is located over that of the remolded treated soil in the figure, therefore, is in a bulky state compared with the remolded one. The non-disturbed treated soil approaches the remolded treated soil asymptotically accompanied with plastic deformation in stress level over the consolidation yield stress. Figure 2 shows oedometer test results of a naturally deposited clay obtained at *Urayasu*, Japan and the remolded it. By comparing Figure 1 and 2, we can find that treated soils and naturally deposited clays share common mechanical features. In Figure 1, the state of the remolded un-treated soil is located more under that of the remolded treated soil. This relationship indicates that the reference state of a treated soil is decided by not the remolded un-treated soil but the remolded treated soil. In addition, the remolded treated soil shows almost linear compression behavior although that is different from the remolded un-treated soil. We also find that remolded treated soils exhibit similar mechanical behavior with remolded un-treated soils.

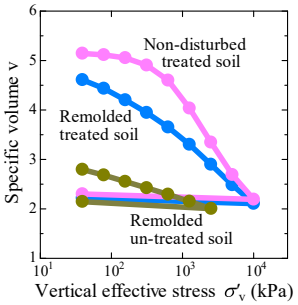

Figure 1. Oedometer tests for a cement-treated soil.

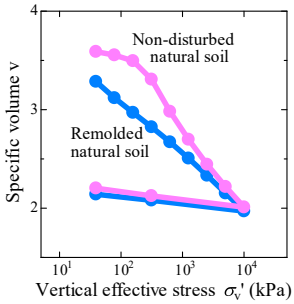

Figure 2. Oedometer tests for a naturally deposited clay.

2 .3 *Undrained tiraxial shear test*

Figure 3 shows undrained shear behaviors of the non-disturbed treated soil. The critical state line (CSL) obtained from undrained shear tests for the remolded treated soil is illustrated in the figure. For comparison, undrained shear behaviors of the

naturally deposited clay obtained from *Urayasu* are shown in Figure 4. We can also find that non-disturbed treated soils exhibit similar behavior with naturally deposited clays in a broader perspective. Especially, softening behavior with plastic volumetric compression and/or with decrease in mean effective stress, which typical naturally deposited clays often show when degrading soil structure, can be seen in Figure 3. The non-disturbed treated soil approaches the CSL obtained from tests for the remolded treated soil asymptotically. Figure 3 also indicates that the reference state of a treated soil is given by the remolded treated soil. The mechanical features mentioned above insist that the soil skeleton structure concept that was applied by Asaoka et al. (2002) to produce the SYS Cam-clay model is valid for treated soils.

On the other hand, mechanical features that naturally deposited clays do not have can be seen in Figure 3. That is plastic volumetric compression (i.e. decrease in mean effective stress under undrained condition) above the CSL. We can easily confirm while mean effective stress decreases only below the CSL in Figure 4, such phenomenon occurs even above the CSL in Figure 3. Note that some effective stress paths of the treated soil reach to the so-called zero-tension cut line ($q = 3p'$), which is illustrated in Figure 3. If a mean effective stress path reaches the line, the undrained condition is broken because pore water can leak between the membrane and the specimen. We need to pay attention to the point when looking at the results of treated soils.

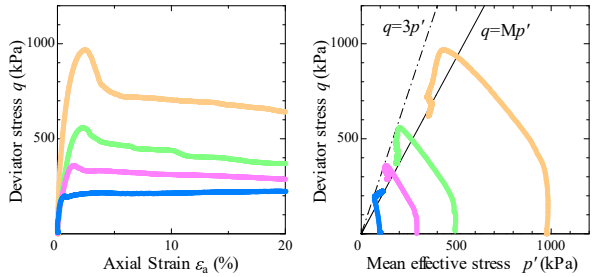

Figure 3. Undrained tiraxial tests for a non-disturbed treated soil.

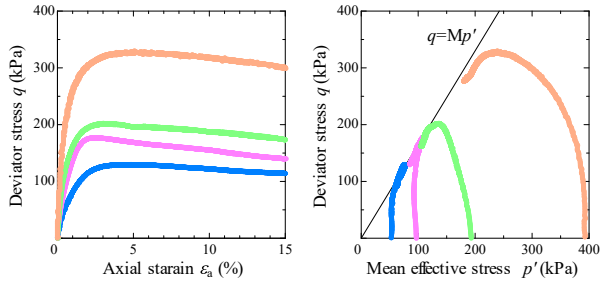

Figure 4. Undrained tiraxial tests for a non-disturbed naturally deposited clay.

3 EXPANSION OF SYS CAM-CLAY MODEL

In this section, we will expand the SYS Cam-clay model based on the above mentioned experimental facts to simulate the mechanical behavior of cement-treated soils.

3 .1 *Outline of expansion*

The expansion introduced to SYS Cam-clay model consists of the following three key points.

Firstly, three loading surfaces (normal yield surface, superloading surface and subloading surface) are translated in the negative direction along the p' axis as shown in Figure 5. Some of the previous studies on constitutive models for cement treated soils have selected a similar kind of method (Gens and Nova 1993, Kasama et al. 2000). This expansion realizes a simple idea of giving the cohesion to a base model. As shown in a later section, this expansion enables plastic compression behavior above the CSL.

Secondly, we will assume that the translation of the loading surfaces restitutes accompanied with plastic deformation. This expansion is based on the experimental fact that treated soils approach the remolded state asymptotically under loading condition, and remolded treated soils exhibit similar behavior with remolded naturally deposited clays. Therefore, the proposed model comes down to the original SYS Cam-clay model accompanied with plastic deformation due to the effect of the second key point.

Finally, the proposed model is described using the modified stress that is defined by subtracting the quantity of translation ($\boldsymbol{\alpha}$ in Figure 5) from the current effective stress $\boldsymbol{T}'$ (extension is positive). If no treatment is applied, the mean effective stress p' can be negative due to the translation. Since Cam-clay model is based on the $\mathrm{v} - \ln p'$ linear relationship (where v is specific volume), it causes a trouble. Therefore, this expansion is useful to maintain the parameter of logarithm in positive. The adaption of this modified stress is also fundamental for the proposed model to be able to come down to the original SYS Cam-clay model.

In the following section, after the proposed model is described using the modified stress based on the first and third key points, the evolution rule of $\boldsymbol{\alpha}$, which represents the modified origin, is provided to realize the second key point. Note that, in the following discussion, $\boldsymbol{D}$ represents stretching (expansion is positive), and the additive decomposition of $\boldsymbol{D}$ into the elastic component $\boldsymbol{D}^e$ and the plastic component $\boldsymbol{D}^p$ is assumed.

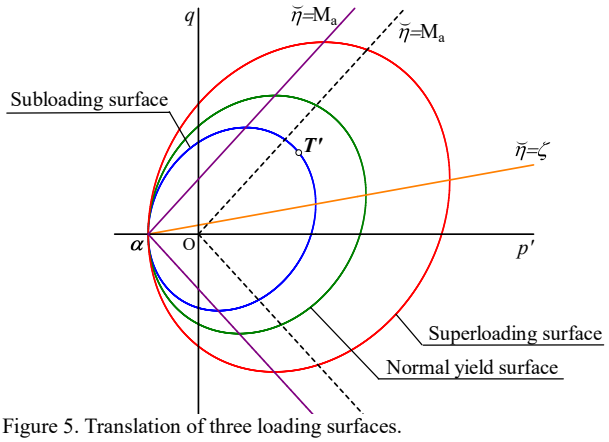

Figure 5. Translation of three loading surfaces.

3 .2 *SYS Cam-clay model described by using the modified stress*

(a) Definition of modified stress (modification of effective stress): The modified stress $\breve{\boldsymbol{T}}'$ is defined as follows:

$$\breve{\boldsymbol{T}}' = \boldsymbol{T}' - \boldsymbol{\alpha} \,. \tag{1}$$

In the proposed model, $\breve{\boldsymbol{T}}'$ plays a role as the effective stress for treated soils.

(b) Subloading surface: The subloading surface of the proposed model is described by introducing the modified stress $\breve{\boldsymbol{T}}'$ as follows:

$$\begin{aligned} &f(\breve{p}', \breve{\eta}^*) + \mathrm{MD}\ln R^* + \mathrm{MD}\ln R + \int_0^t J\,\mathrm{tr}\boldsymbol{D}^p d\tau = 0, \\ &f(\breve{p}', \breve{\eta}^*) = \mathrm{MD}\ln\frac{\breve{p}'}{\widetilde{p}'_{c0}} + \mathrm{MD}\ln\frac{\mathrm{M}^2 + \breve{\eta}^{*2}}{\mathrm{M}^2}, \end{aligned} \tag{2}$$

where $\mathrm{D} = (\widetilde{\lambda} - \widetilde{\kappa})/\mathrm{Mv}_0$, $J = \mathrm{v}/\mathrm{v}_0$. $\widetilde{p}'_{c0}$ represents the magnitude of the initial normal yield surface. $\widetilde{\lambda}$, $\widetilde{\kappa}$ and M

are the compression index, the swelling index and the critical state constant, respectively. Several stress components and invariants are defined as follows: $\breve{p}' = -(1/3)\breve{\boldsymbol{T}}'$, $\breve{\eta}^* = \| \hat{\boldsymbol{\eta}} \|$, $\hat{\boldsymbol{\eta}} = \breve{\boldsymbol{\eta}} - \boldsymbol{\beta}$, $\breve{\boldsymbol{\eta}} = \breve{\boldsymbol{s}} / \breve{p}'$, $\breve{\boldsymbol{s}} = \breve{\boldsymbol{T}}' + \breve{p}'\boldsymbol{I}$, where $\boldsymbol{\beta}$ is the back stress to rotate the three loading surfaces. R^* is the ratio of the size of the normal yield surface to that of the superloading surface, and R is the ratio of the size of the normal yield surface to that of the superloading surface. The similarity center of each surface is located on α. $\boldsymbol{\alpha}$ and $\boldsymbol{\beta}$ introduce the cementation effect and the induced anisotropy to the model, respectively. The reciprocals of $R^*$and R represent the degree of structure and the overconsolidation ratio, respectively.

(c) Elastic constitutive model: The following confining pressure dependent rate type Hooke's law using $\breve{p}'$ instead of p' is used as the elastic constitutive model:

$$\overset{\circ}{\breve{\boldsymbol{T}}}' = \boldsymbol{E}\boldsymbol{D}^{\mathrm{e}} = \left(\widetilde{K} - \frac{2}{3}\widetilde{G} \right)\left(\mathrm{tr}\boldsymbol{D}^{\mathrm{e}}\right)\boldsymbol{I} + 2\widetilde{G}\boldsymbol{D}^{e}, \quad \widetilde{K} = \frac{J\,\mathrm{v}_0}{\widetilde{\kappa}}\breve{p}', \quad \widetilde{G} = \frac{3(1-\nu)}{2(1+\nu)}\widetilde{K}, \tag{3}$$

where ν is the Poisson's ratio. $\overset{\circ}{(\,)}$ represents a co-rotation rate.

(d) Associated flow rule: When the subloading surface is selected as the plastic potential, the following associated flow rule in the modified stress space is adopted:

$$\boldsymbol{D}^{p} = \Lambda \frac{\partial f}{\partial \breve{\boldsymbol{T}}'}, \quad (\Lambda > 0), \tag{4}$$

where Λ is called the plastic multiplier.

(e) Evolution rule of R^*, R, $\boldsymbol{\beta}$: Evolution rules of R^*, R and $\boldsymbol{\beta}$ are given by the following equations:

$$\dot{R}^* = JU^* \left\{ (1-c_s)(-D_v^p) + c_s\sqrt{\frac{2}{3}}\left\|\boldsymbol{D}_s^p\right\| \right\}, \quad U^* = \frac{a}{\mathrm{D}} R^{*b}(1-R^*)^c; \tag{5}$$

$$\dot{R} = JU\left\|\boldsymbol{D}^p\right\|, \quad U = -\frac{m}{\mathrm{D}}\ln R; \tag{6}$$

$$\overset{\circ}{\boldsymbol{\beta}} = J\frac{b_r}{\mathrm{D}}\sqrt{\frac{2}{3}}\left\|\boldsymbol{D}_s{}^p\right\| \left\|\breve{\boldsymbol{\eta}}^*\right\| \breve{\boldsymbol{\eta}}_b, \quad \breve{\boldsymbol{\eta}}_b = m_b \frac{\breve{\boldsymbol{\eta}}^*}{\left\|\breve{\boldsymbol{\eta}}^*\right\|} - \boldsymbol{\beta}; \tag{7}$$

where $D_v^p = \mathrm{tr}\boldsymbol{D}^p$, $\boldsymbol{D}_s^p = \boldsymbol{D}^p - (1/3)(\mathrm{tr}\boldsymbol{D}^p)\boldsymbol{I}$ and a, b, c, c_s, m, m_b, b_r are material constants.

(f) Plastic multiplier: The plastic multiplier Λ is derived from substituting Eqs. (3), (4), (5), (6) and (7) into the consistency condition of Eq. (2) as follows:

$$\Lambda = \frac{\dfrac{\partial f}{\partial \breve{\boldsymbol{T}}'} \cdot \boldsymbol{E}\boldsymbol{D}}{J\dfrac{\mathrm{MD}}{(\mathrm{M}^2 + \breve{\eta}^{*2})\breve{p}'}(\mathrm{M}_s{}^2 - \breve{\eta}^2) + \dfrac{\partial f}{\partial \breve{\boldsymbol{T}}'} \cdot \boldsymbol{E}\dfrac{\partial f}{\partial \breve{\boldsymbol{T}}'}}, \tag{8}$$

where

$$\mathrm{M}_s{}^2 = \mathrm{M}_a{}^2 + 3\breve{p}'\breve{\boldsymbol{\eta}} \cdot \boldsymbol{b} - (\mathrm{M}^2 + \breve{\eta}^{*2})\breve{p}'\left(\frac{r^*}{R^*} - \frac{r}{R} \right), \tag{9}$$

$$\mathrm{M}_a{}^2 = \mathrm{M}^2 + \xi^2, \quad \xi^2 = \sqrt{3/2}\left\|\boldsymbol{\beta}\right\|, \tag{10}$$

and r^*, r, $\boldsymbol{b}$ satisfies $\dot{R}^* = \Lambda J r^*$, $\dot{R} = \Lambda J r$, $\overset{\circ}{\boldsymbol{\beta}} = \Lambda J \boldsymbol{b}$. $\breve{\eta}^2 = \mathrm{M}_s{}^2$ and $\breve{\eta}^2 = \mathrm{M}_a{}^2$ work as the threshold lines between hardening and softening, plastic volumetric compression and expansion, respectively.

(g) Elasto-plastic constitutive model: The following equation is obtained by substituting $\boldsymbol{D}^e = \boldsymbol{D} - \boldsymbol{D}^p$ and Eq. (4) into Eq. (3).

$$\overset{\circ}{\breve{\boldsymbol{T}}}' = \boldsymbol{E}\boldsymbol{D} - \Lambda\boldsymbol{E}\frac{\partial f}{\partial \breve{\boldsymbol{T}}'} \tag{11}$$

(h) Loading criteria: Loading criteria is given as follows on the condition that the denominator of Eq. (8) is always positive.

$$[1]\ \frac{\partial f}{\partial \breve{\boldsymbol{T}}'} \cdot \boldsymbol{E}\boldsymbol{D} > 0 \ :\ \boldsymbol{D}^p \neq \boldsymbol{0} \quad \text{(Loading)} \tag{12a}$$

$$[2]\ \frac{\partial f}{\partial \breve{\boldsymbol{T}}'} \cdot \boldsymbol{E}\boldsymbol{D} \leq 0 \ :\ \boldsymbol{D}^p = \boldsymbol{0} \quad \text{(Unloading)} \tag{12b}$$

(i) State equation: The state variables always satisfy the following equation when the initial values of them are given to satisfy the equation.

$$\mathrm{v} = \mathrm{N} - \widetilde{\lambda}\ln\breve{p}' - (\widetilde{\lambda} - \widetilde{\kappa})\ln\frac{R^*}{R}\frac{\mathrm{M}^2 + \breve{\eta}^{*2}}{\mathrm{M}^2}, \tag{13}$$

where N is the intercept of the NCL.

The above formulation is as same as that of the SYS Cam-clay model except for replacing the effective stress $\boldsymbol{T}'$ with $\breve{\boldsymbol{T}}'$. As a result, a relationship between the co-rotation rate of $\breve{\boldsymbol{T}}'$ and $\boldsymbol{D}$ is obtained as shown Eq. (11). We need to convert the equation into a relationship between the co-rotation rate of $\boldsymbol{T}'$ and $\boldsymbol{D}$. An evolution rule of $\boldsymbol{\alpha}$ enables that as shown the following subsection.

3 .3 *Degradation of cementation and true effective stress rate*

(j) Evolution rule of $\boldsymbol{\alpha}$: $\boldsymbol{\alpha}$ satisfies the following equation since it is on the p' axis.

$$\boldsymbol{\alpha} = \Psi\boldsymbol{I}, \quad \Psi = \frac{1}{3}\mathrm{tr}\boldsymbol{\alpha} \tag{14}$$

where Ψ represents the magnitude of the translation of the three loading surfaces from the origin of the stress space and introduces the cementation effect to the model. This state variable has the same unit with stress. Ψ should gradually decrease to zero during loading condition based on the experimental fact that the cementation effect disappears due to plastic deformation. The following simple evolution rule of Ψ is given as follows:

$$\dot{\Psi} = JV\left\|\boldsymbol{D}^p\right\|, \quad V = -\frac{d}{D}\Psi, \tag{15}$$

where $V(\Psi)$ is a monotonically decreasing function of Ψ and satisfies $V(0) = 0$. d is the material constant that controls the decreasing rate of Ψ and is called the degradation index of cementation. The co-rotational rate of $\boldsymbol{\alpha}$ is given as follows:

$$\overset{\circ}{\boldsymbol{\alpha}} = \dot{\Psi}\boldsymbol{I}. \tag{16}$$

(g') Constitutive equation: By substituting Eq. (16) into Eq. (11), a relationship between $\boldsymbol{T}'$ and $\boldsymbol{D}$ is obtained as follows:

$$\overset{\circ}{\boldsymbol{T}}' = \overset{\circ}{\breve{\boldsymbol{T}}}' + \overset{\circ}{\boldsymbol{\alpha}} = \boldsymbol{E}\boldsymbol{D} - \Lambda\left(\boldsymbol{E}\frac{\partial f}{\partial \breve{\boldsymbol{T}}'} - J\psi\boldsymbol{I} \right), \tag{17}$$

where ψ satisfies $\dot{\Psi} = \Lambda J\psi$. Even though the definition of the effective stress was modified, Eq. (17) does not demand radical change to the basic algorism of several numerical analysis codes for solving initial boundary value problems when adopting the proposed model to the codes.

4 SIMULATION OF ELEMENT TESTS BY USING THE PROPOSED MODEL

In this section, we will demonstrate some simulations of the element tests for the cement-treated soil shown in Section 2 to validate the proposed model.

4 .1 *Analysis conditions*

Table 2 shows material constants and initial values for the non-disturbed treated soil. The elasto-plastic parameters were basically decided from test results of the remolded treated soil. In order to verify the effect of expansion, the case with

cementation was compared with the case without cementation. The initial overconsolidation ratios were calculated from the other initial values by using Eq. (13).

Table 2. Material constants and initial values.

Elasto-plastic parameters			
Compression index	λ	0.590	
Swelling index	κ	0.050	
Critical state constant	M	1.850	
NCL interception	N	4.700	
Poisson's ratio	ν	0.300	
Evolution parameters			
Degradation index of overconsolidation	m	1	
Degradation indices of structure	a	0.4	
(b=c=1.0)	c_s	0.4	
Rotational hardening index	b_r	0.1	
Limitation of rotational hardening	m_b	0.35	
Degradation index of cementation	d	0.0015	
Initial values		With cementation	Without cementation
Overconsolidation ratio	$1/R_0$	2.8	57.8
Degree of structure	$1/R^*_0$	10.0	10.0
Vertical effective stress	σ'_{v0}	10.0	10.0
Specfic volume	v_0	5.1	5.1
Stress ratio	η_0	0.0	0.0
Anisotropy	ζ_0	0.0	0.0
Cementation (kPa)	Ψ_0	150.0	0.0

4 .2 *Simulation of oedometer test*

Figure 6 shows simulations of the oedometer tests for the non-disturbed and remolded treated soils. When conducting the simulation for the remolded treated soil, the initial degrees of structure $1/R^*_0$ and cementation Ψ_0 are set to 1.0. The pale bold lines represent experimental results, and the deep fine lines represent simulations (Fig. 7 is also the same). Both the simulations capture well the features of the experiments. These figures insist the cementation effect hardly appear in the oedometer tests while the structure and overconsolidation remarkably affect the one dimensional compression behavior. This is because the effect of the translation of three loading surfaces relatively diminish according to increase in stress level and hardly appear under low stress ratio.

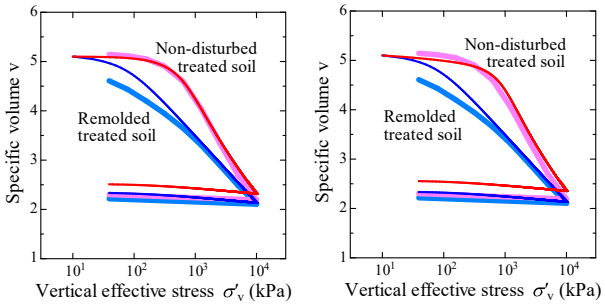

(a) With cementation (b) Without cementation

Figure 6. Simulations of oedometer tests. (Pale bold line: experiment, deep fine line simulation)

4 .3 *Simulation of Undrained Shear Test*

Figure 7 shows simulations of the undrained tiraxial shear tests for the non-disturbed treated soil. Each simulation for the tiraxial tests includes the calculation of the consolidation process. In spite of the presence of absence of the cementation, the simulations exhibit softening behavior with plastic volumetric compression and hardening behavior with plastic volumetric expansion, which the simple Cam-clay model cannot reproduce. These behaviors are also produced due to the effects of structure and overconsolidation. On the other hand, only the case with cementation exhibits plastic volumetric compression (decrease in mean effective stress under undrained condition) above the CSL. In the case with cementation, effective stress paths reach high stress ratio. However, even in the case with cementation, simulations under the confining pressures of 100 and 300 kPa are different from experiments in high stress ratio level. This is because the effective stress paths of the simulations exceed the zero-tension cut line ($q = 3p'$), which is a limit of tiraxial test. In the case with cementation, initial shear stiffness is high under low confining pressure as well as the experiments. This is the effect of the application of the modified effective stress. Although deviator stress of experiments decreases rapidly in q-ε_a relationship compared with simulations. We think that this difference is not important for the simulation as an element because the rapid decreasing of q must be the influence of strain localization.

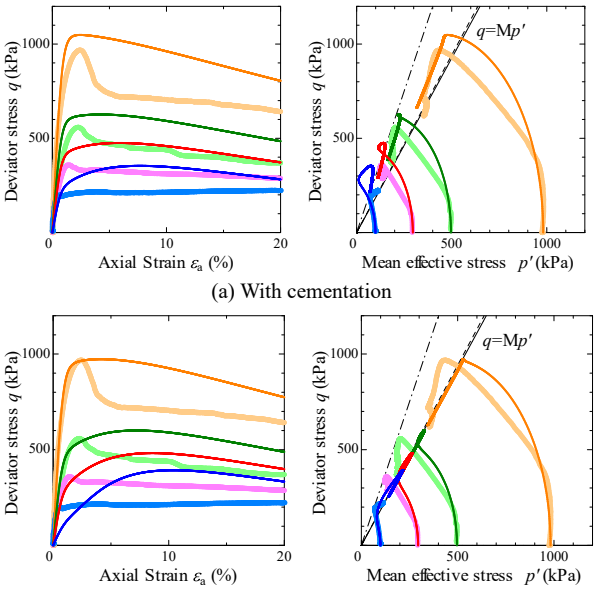

(a) With cementation

(b) Without cementation

Figure 7. Simulations of undrained tests. (Pale bold line: experiment, deep fine line: simulation)

5 CONCLUSION

This study expanded the SYS Cam-clay model based on element experiments of a cement-treated soil. The proposed model enables simulation of the mechanical behavior of cement-treated soils as shown in this paper.

6 ACKNOWLEDGEMENTS

The authors deeply appreciate Prof. Toshihiro Noda of Nagoya University for his support in the present study. This study was also supported by JSPS KEKENHI Grant Number JP16H04408.

7 REFERENCES

Asaoka, A., Noda, T., Yamada, E., Kaneda, K. and Nakano, M. 2002. An elasto-plastic description of two distinct volume change mechanisms of soils, *Soils and Foundations*, 42(5), 47-57.

Coastal development institute of technology. 2008. Manual of the pneumatic flow mixing method, Coastal technique library, No.32, (in Japanese).

Gens A. and Nova R. 1993. Conceptual bases for a constitutive model for bonded soils and weak rocks, *Proc. 1st Int. Conf. Hard Soils and Soft Rocks*, 485-494.

Kasama K. Ochiai H. Yasufuku H. 2000. On the stress-strain behaviour of lightly cmeneted clay based on an extended critical state concept, *Soils and Foundations*, 40(5), 37-47.